Theoretical Analysis of Infrared Radiation Shields of Spacecraft

David L. Shealy*
University of Alabama in Birmingham, University Station, Alabama

For a system of N diffuse, gray body radiation shields which view only adjacent surfaces and space, the net radiation method for enclosures has been used to formulate a system of linear, nonhomogeneous equations in terms of the temperatures to the fourth power of each surface in the coupled system of enclosures. The coefficients of the unknown temperatures in the system of equations are expressed in terms of configuration factors between adjacent surfaces and the emissivities. As an application, a system of four conical radiation shields for a spin stabilized STARPROBE spacecraft has been designed and analyzed with respect to variations of the cone half angles, the intershield spacings, and emissivities.

Nomenclature

a_i = absorptivity of surface i
A_i = total area of surface i
dA_i = element of area of surface i
$D_{i-1,i}$ = axial spacing between adjacent shield surfaces $i-1$ and i
E_{bi} = the total black body emissive power density of surface i, σT_i^4
$F_{i\to j}$ = the fraction of energy emitted by surface i and incident upon surface j (configuration factor)
G_i = the irradiation of surface i, the power per unit area incident upon surface i
J_i = the radiosity of surface i, the power per unit area leaving surface i
$M(i,j), N(i)$ = coefficients in Eq. 5
$Q_{\text{in}}(i), Q_{\text{out}}(i)$ = the total power incident upon and leaving surface i
$(r_i, \phi_i z_i)$ = cylindrical coordinates of surface i
T_i = temperature of surface i
$Z_{0,i}$ = axial intercept coordinate for the apex of shield surface i
α_i = cone half angle of shield surface i
ϵ_i = emissivity of surface i
ρ_i = reflectivity of surface i
σ = Stefan-Boltzmann constant, 5.67×10^{-8} w/m^2 K^4

Introduction

RECENTLY there has been considerable interest in sending an unmanned spacecraft, known as STARPROBE, to a distance of a few solar radii from the sun.[1-3] During the past few years, a mission-option study for STARPROBE has been carried out. Reference 4 presents a detailed overview for the scientific objectives, trajectory, and mission design for STARPROBE.

In order for the spacecraft to survive the near solar environment of four solar radii from the center of the sun at perihelion, STARPROBE will require a radiation shield system which is capable of withstanding solar thermal fluxes about 3000 times higher than outside the atmosphere of the Earth, and which also prevents the bulk temperature of the spacecraft payload from exceeding 55°C (328°K). The fundamental configuration of the radiation shield system consists of a primary thermal shield and one or more secondary infrared shields. The primary thermal shield should be capable of withstanding the high solar flux, and will cast a shadow over the secondary shields and payload. As a result of the large angular diameter of the sun (approximately equal to 28.96 deg) at perihelion, the primary shield's shadow will be conical in shape. The outer diameter of the primary shield is currently limited by the launch vehicle (4.06 m for the cargo bay of the Space Shuttle). Reference 5 provides a detail specification of the design requirements for the primary thermal shield of STARPROBE.

The primary thermal shield can accommodate the high thermal fluxes during the solar encounter by reflection or emission, rather than storage. However, a major problem with reflective systems is the uncertainty of the effects of the solar winds on the specular properties of the reflectors.[6,7] Also, surface changes due to displacement damage at high temperatures tend to lower the total reflectances. Normally, materials which can withstand such high temperatures have reflectances of the order of 0.6 or less (see Table 1). Various authors[8-10] have investigated the feasibility of using an emissive system for the primary thermal shield which would be in thermal equilibrium with the solar flux and the reradiation of the incident energy back into space. Preliminary studies indicate that the primary thermal shield would have a temperature in the range of 1900 to 2500°K, depending on the geometry and material used.

For the present study, it is assumed that an emissive based primary thermal shield has been designed and has a specified shape, emissivity, and equilibrium temperature. However, it is recognized that in practice the radiative heat transfer between the primary and secondary shields is a coupled process, preventing specification of a surface temperature. The primary sheild temperature has been assumed to be fixed in this study within realistic limits in order to simplify the analysis of the secondary shield system. The purpose of this work is to demonstrate a solution technique for evaluating secondary shield configurations for which the temperature of the payload remains less than 55°C during solar encounter and to determine the temperature levels and emissivities for each secondary shield and payload. In order to obtain a solution of this problem, the net-radiation method[11-13] has been formulated for the STARPROBE spacecraft, assuming all surfaces are diffuse, gray body emitters in equilibrium such that Kirchhoff's law holds at each surface.

Received March 21, 1983; revision received Aug. 26, 1983.

*Associate Professor of Physics. Member AIAA.

It is conventional to design a system of radiation shields based on the assumption that each shield is an infinite plane,[14,15] thus reducing the complexity introduced by configuration factors. Reference 8 reports a design technique for the heat shields of STARPROBE, assuming all surfaces are black body radiators and the secondary shields are coaxial disks which are spaced such that the ratio of the radius of a disk to the spacing between disks is constant. The general formulation of the net-radiation method for the thermal analysis of the gray body secondary shields of the spacecraft in this study depends upon the configuration factors between adjacent surfaces. Thus, the formulation of the net-radiation method presented is applicable to the design of an arbitrary system of gray body secondary radiation shields. Specific application of these general results is given for a spin stabilized STARPROBE spacecraft with conical shaped radiation shields with arbitrary apex angles and axial spacings.

Net Radiation Method for Radiation Shields

For the present analysis, the secondary shields and spacecraft payload are considered only as reradiative surfaces. That is, the net power flow to each secondary shield and the spacecraft payload is zero

$$Q_{\text{net}}(i) = Q_{\text{in}}(i) - Q_{\text{out}}(i) = 0 \tag{1}$$

where $i = 1,2,\ldots,N$ for the secondary shields and $i = N+1$ or SC for the spacecraft payload. A symbolic diagram of the spacecraft heat shield system is given in Fig. 1.

In heat transfer calculations at surface i, it is important to recognize that for gray surfaces, a portion of the incident radiation is reflected and must be accounted for in the energy balance. Also, for diffuse gray surfaces in equilibrium, the surface emissivity is equal to its absorptivity (Kirchhoff's Law, Ref. 12). So, for an opaque surface i, one has

$$a_i = \epsilon_i = 1 - \rho_i \tag{2}$$

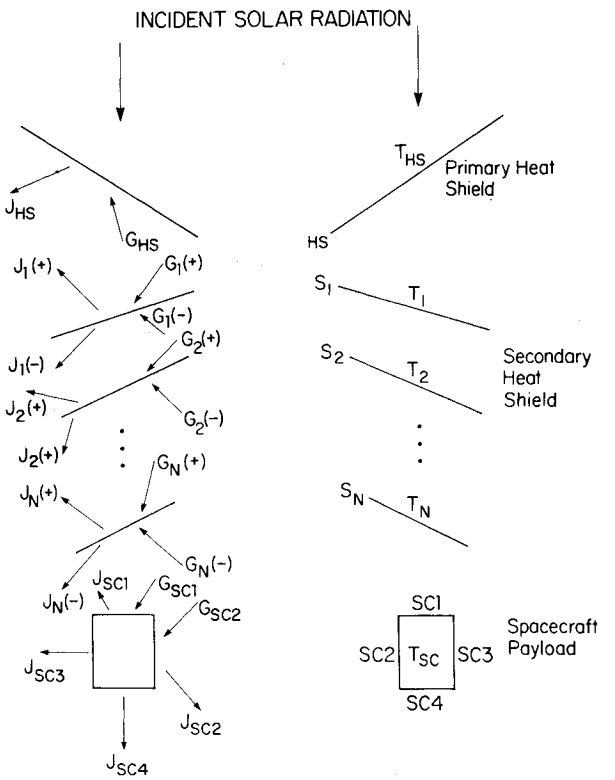

Fig. 1 Symbolic diagram for a cross-section of the STARPROBE spinner spacecraft.

If surface i is assumed to be infinitely thin (neglecting conductivity) and to be at a constant temperature, then the energy balance at surface i is given by

$$A_i[G_i(+)G_i(-)] = [J_i(+) + J_i(-)]A_i \tag{3}$$

where $G_i(+)$ and $G_i(-)$ are the irradiations of the upper and lower side for surface i. $J_i(+)$ and $J_i(-)$ are the radiosities for the upper and lower sides of surface i and are given by

$$J_i(+) = \epsilon_i E_{bi} + \rho_i G_i(+) \tag{4a}$$

$$J_i(-) = \epsilon_i E_{bi} + \rho_i G_i(-) \tag{4b}$$

An implicit assumption, which has been made in Eqs. (4a) and (4b), is that

$$\epsilon_i(+) = \epsilon_i(-) \equiv \epsilon_i \tag{4c}$$

Equation (4c) is consistent with a thin secondary shield surface model where neither side of the surface has been coated.

Imposing the energy balance, Eq. (3), at each surface gives a system of $N+1$ linear, nonhomogeneous equations in E_{bi} for the N secondary shields and the spacecraft surface

$$\begin{aligned}
&M(1,1)E_{b1} + M(1,2)E_{b2} &&= N(1)E_{bHS}\\
&M(2,1)E_{b1} + M(2,2)E_{b2} + M(2,3)E_{b3} &&= 0\\
&+M(3,2)E_{b2} + M(3,3)E_{b3} + M(3,4)E_{b4} &&= 0\\
&\quad\vdots \qquad\qquad \vdots \qquad\qquad \vdots\\
&+M(N,N-1)E_{bN-1} + M(N,N)E_{bN}\\
&\quad +M(N,N+1)E_{bSC} &&= 0\\
&+M(N+1,N)E_{bN} + M(N+1,N+1)E_{bSC} &&= 0
\end{aligned} \tag{5}$$

See Appendix A for a derivation of Eq. (5) and explicit expressions for the coefficients $M(i,j)$ and $N(1)$. The system of Eq. (5) can be solved by conventional matrix techniques[16] for the $N+1$ unknown emissive powers. Then the temperatures

Table 1 Emittance as a function of temperature

Material	Temperature (°K)	Hemispherical emittance
Tantalum	500	0.10
	1200	0.15
	1700	0.21
	2200	0.25
	2900	0.30
Tungsten	1000	0.10
	1600	0.21
	1900	0.25
	2400	0.30
	3000	0.33
Titanium	500	0.180
	800	0.225
	1200	0.275
	1400	0.300
	1800	0.340
Incone	673	0.504
	773	0.547
	873	0.584
	1073	0.643
	1273	0.690

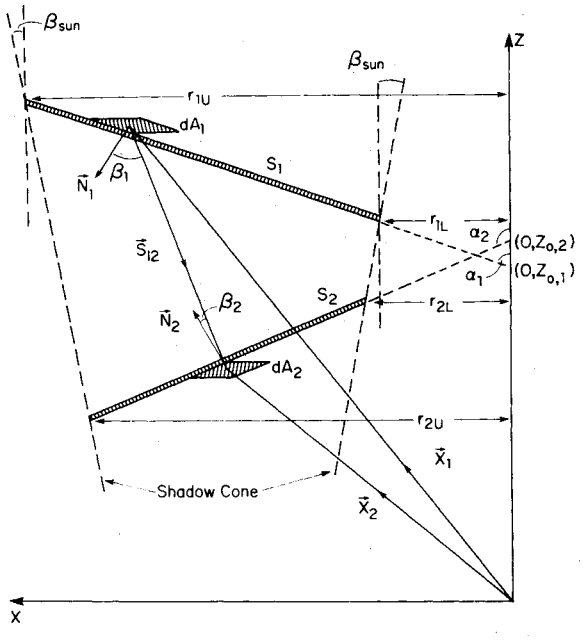

Fig. 2 Positive x-z cross-section of the radiation shield surfaces S_1 and S_2.

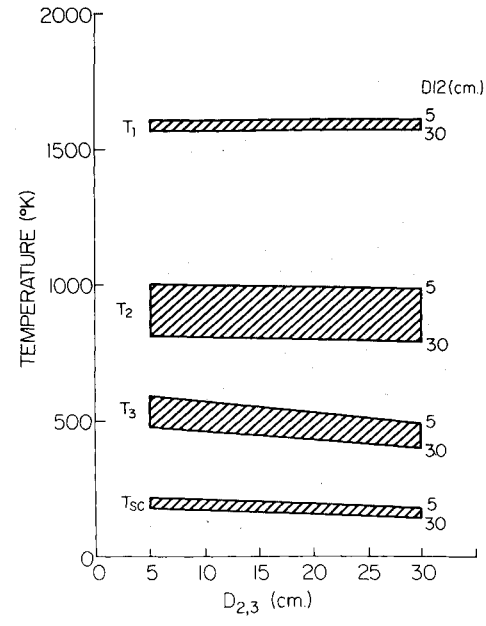

Fig. 3 Secondary heat shield and payload temperatures vs $D_{2,3}$ for $T_{HS}=2100°K$, $E_1=E_2=E_3=0.1$, $D_{HS}=5$ cm, $\alpha_1=100°K$, $\alpha_2=105°$, $\alpha_3=110°$.

for each surface is given by

$$T_i=[E_{bi}/\sigma]^{1/4}, i=1,2,\ldots,N,SC \tag{6}$$

Equations (5) and (6) provide deterministic relationships between shield temperatures and the emissivities, geometrical shape, and orientation parameters for the shield surfaces. These results can be used to generate parametric curves of the surface temperatures vs the design parameters for arbitrary shield shapes and orientations, provided the heat shields view only adjacent surfaces and space. The shield configuration factors, $F_{i\to i}$, have been neglected in this analysis, since adjacent surface configuration factors, $F_{i\to j}$, are much larger than the self view configuration factors, $F_{i\to j}$, due to the close proximity of adjacent shield surfaces. It should also be noted that the present work is an extension of the conventional N body enclosure problem[17,18] to that of $N+1$ coupled four body enclosures, since it has been assumed that adjacent shield surfaces only view each other and space. As an application, Eqs. (5) and (6) have been programmed for N conical secondary shields for the STARPROBE spinner spacecraft system such that when the design parameters are varied, the temperatures for each secondary shield surface and the spacecraft are obtained.[19]

Application to STARPROBE Spacecraft

In order to illustrate how Eq. (5) is used to design the secondary heat shields of a spacecraft, assume that the primary and secondary heat shield surfaces for a STARPROBE spinner spacecraft are conical and satisfy the equation of the surfaces

$$Z=Z_0+r\cot\alpha \tag{7}$$

where Z_0 specifies the apex location, α gives the cone half angle of the surface measured from the positive Z direction, and r is the radial distance from the symmetry axis to a point on the surface. Figure 2 displays the positive X-Z section of the primary heat shield, which is labeled by the subscript 1, and of the first secondary shield, which is labeled by the subscript 2. In the present model, α_1 for the primary shield is fixed at 60 deg, and the cone half angles, α_i, for the secondary shields can vary from 0 to 180 deg.

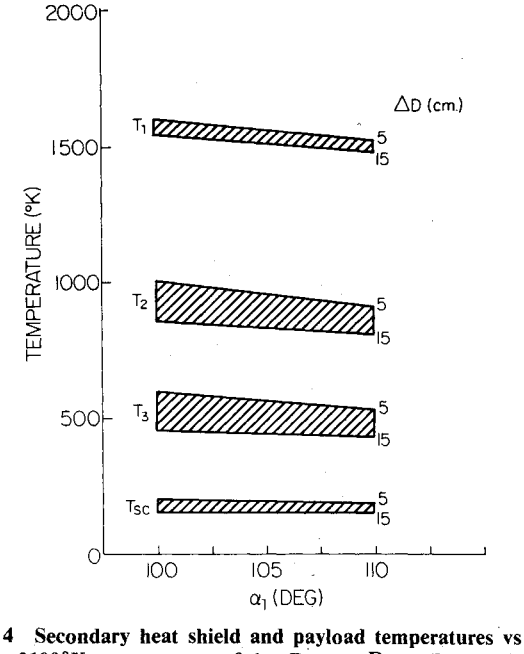

Fig. 4 Secondary heat shield and payload temperatures vs α_1 for $T_{HS}=2100°K$, $\epsilon_1=\epsilon_2=\epsilon_3=0.1$, $D_{HS,1}=D_{1,2}=D_{2,3}=\Delta D$, $\alpha_2=\alpha_1+5°$, $\alpha_3=\alpha_1+10°$.

In order to evaluate the coefficients in Eq. (5), it is necessary to evaluate the configuration factors between adjacent shield surfaces. Appendix B presents formulas for the necessary configuration factors. With these results, numerical integrations over the radiation shield surfaces are performed in computing the configuration factors between adjacent surfaces. The linear, nonhomogeneous system of Eq. (5) are then solved for the emissive power density of each surface. During the deisgn process, these calculations are repeated many times for different variables. Therefore, it is desirable to use numerical algorithms which are as fast as possible while providing the necessary accuracy. It has been found[19] that the double precision, 16-point Gaussian

quadrature, DQG16,[20] yields temperature values to within a few percent accuracy.

Now, consider the spinner STARPROBE spacecraft illustrated in Fig. 1 with three secondary shields and defined by the system parameters

Primary Shield

$$r_{HS}=0.711\text{ m} \qquad \alpha_{HS}=60\text{ deg}$$

$$R_{HS}=2.032\text{ m} \qquad T_{HS}=2100^\circ\text{ K}$$

$$H_{HS}=0.762\text{ m} \qquad \epsilon_{HS}=0.8 \tag{8a}$$

Primary Shield to Payload Distance

$$D_{HS-SC}=0.965\text{ m} \tag{8b}$$

Payload

$$r_{SC}=1.105\text{ m}$$

$$R_{SC}=1.435\text{ m}$$

$$H_{SC}=0.508\text{ m} \tag{8c}$$

As a first step in the design of the secondary heat shield system, the cone half angles, α_i, and the shield spacings, $D_{i,j}$ were assumed to have the values

$$\alpha_1=100, 105, 110\text{ deg} \qquad D_{HS,1}=5, 10, 15, 20, 30\text{ cm}$$

$$\alpha_2=105, 110, 115\text{ deg} \qquad D_{1,2}=5, 10, 15, 20, 30\text{ cm}$$

$$\alpha_3=110, 115, 120\text{ deg} \qquad D_{2,3}=5, 10, 15, 20, 30\text{ cm} \tag{9a}$$

The emissivities for each secondar shield surface were assumed to be equal and vary as follows

$$\epsilon=\epsilon_1=\epsilon_2=\epsilon_3=1,2,\ldots,8 \tag{9b}$$

The emissivities for the spacecraft payload were assumed to be given by

$$\epsilon_{SC1}=\epsilon_{SC2}=\epsilon_{SC3}=\epsilon_{SC4}=0.015 \tag{9c}$$

The purpose of the variation defined by Eqs. (9a) to (9c) is to analyze the effect of each design variable ($D_{i,j}$; α_i; ϵ_i) on the temperature levels of each secondary heat shield surface and those of the spacecraft payload and to locate an optimum geometrical configuration for the secondary system within this region of parameter space. Then realistic values for the emissivities for each secondary heat shield surface are determined. It should be noted that additional cooling of the spacecraft payload can be obtained by requiring larger values for ϵ_{SC3} and ϵ_{SC4}.

In Fig. 3, the temperature levels for the three secondary heat shield surfaces and the payload are given as a function of the spacing $D_{2,3}$ between shield surfaces S_2 and S_3 as plotted on the abscissa and of the spacing $D_{1,2}$ between S_1 and S_2 as plotted as different curves on the graph. From Fig. 3, one concludes that T_1 and T_2 are almost independent of $D_{2,3}$; T_3 decreases by approximately 20% when either $D_{1,2}$ or $D_{2,3}$ is increased from 5 to 30 cm; T_3 decreases by 33% when $D_{1,2}$ and $D_{2,3}$ are both increased to 30 cm; and T_{SC} decreases by 15% when either $D_{1,2}$ or $D_{2,3}$ is increased to 30 cm. Also T_{SC} decreases by 35% when both $D_{1,2}$ and $D_{2,3}$ are increased to 30 cm. Carrying out similar calculations as presented in Fig. 3 when $D_{HS,1}$ is increased to 15 and 30 cm, one notes that the general dependence of T_2, T_3, and T_{SC} on $D_{1,2}$ and $D_{2,3}$ is similar to that displayed in Fig. 3, except the temperature levels are slightly reduced when $D_{HS,1}$ is increased and T_1 decreases by 5% when $D_{HS,1}$ is increased, from 5 to 30 cm, whereas for given $D_{1,2}$ and $D_{2,3}$, the temperature of the payload, T_{SC}, is not significantly affected by increasing $D_{HS,1}$. These results suggest the optimum intershield spacings are

$$D_{HS,1}\le 10\text{ cm}, \qquad D_{1,2} \text{ and } D_{2,3}\ge 20\text{ cm} \tag{10}$$

Figure 4 gives the temperature levels T_1, T_2, T_3, T_{SC} as a function of the cone half-angle α_1 of S_1 along the abscissa and of the intershield spacing $\Delta D(\equiv D_{HS,1}=D_{1,2}=D_{2,3})$ plotted as different curves. The cone half-angles of S_2 and S_3 are constrained to be given by

$$\alpha_2=\alpha_1+5\text{ deg}, \qquad \alpha_3=\alpha_1+10\text{ deg} \tag{11}$$

The general observations from Fig. 4 are that T_1 decreases by 6% when α_1 is increased from 100 to 110°, with corresponding increases in α_2 and α_3, whereas T_1 decreases only by 3% when ΔD increases from 5 to 15 cm. Also, T_2, T_3, and T_{SC} are stronger functions of ΔD for small α_1 than as a function of α_i's. From similar graphs as Fig. 4, except when α_2 and α_3 are the abscissa, one further concludes that the heat shield temperature T_i is affected most when α_i $(i=2,3)$ is varied, and T_i is a stronger function of ΔD than α_i.

Examining the numerical data of the temperatures vs the system variables defined by Eq. (9) yields the lowest T_{SC} when

$$\alpha_1=100\text{ deg}; \alpha_2=105\text{ deg}; \alpha_3=120\text{ deg}; \bar{\epsilon}=0.1;$$

$$D_{HS,1}=10\text{ cm}; D_{1,2}=30\text{ cm}; D_{2,3}=20\text{ cm} \tag{12}$$

The temperature levels for this "optimum case" geometry are plotted as a function of $\bar{\epsilon}$ in Fig. 5. It is evident from Fig. 5 that T_2, T_3, T_{SC} are strong functions of $\bar{\epsilon}$, with minimum T_i's occuring for minimum $\bar{\epsilon}$'s. It should also be noted from the temperature vs system variables data that the geometrical configuration resulting in minimum T_{SC} is unaffected by specific values of ϵ_1, ϵ_2, ϵ_3.

Having designed a system of three secondary heat shields defined by Eq. (1), realistic values for the emissivities ϵ_1, ϵ_2, ϵ_3 are determined by interpolating the temperature levels of each secondary shield from Fig. 5 with the emissive vs temperature data for several candidate shield materials given in Table 1. Based on the data given in Table 1, tantalum will be a

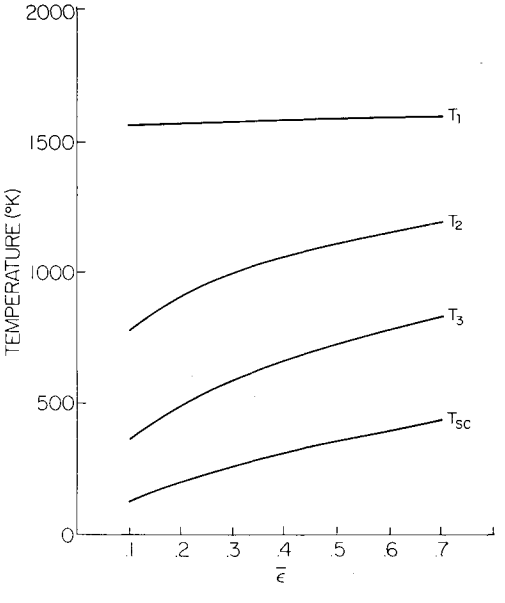

Fig. 5 Secondary heat shield and payload temperature for "optimum case" configuration defined by Eq. (12) vs $\bar{\epsilon}\neq\epsilon_1=\epsilon_2=\epsilon_3$.

suitable thermal material to construct the secondary heat shields and the emissivities of secondary shields for $T_{HS}=2100°K$ are given by

$$\epsilon_1=0.19, \qquad \epsilon_2=0.135, \qquad \epsilon_3=0.1 \tag{13}$$

It should be noted from Table 1 that emissive data for tungsten at temperatures less than 1000°K are not given, but could be extrapolated to be less than the emittance values of tantalum. This suggests that tungsten would, in fact, provide lower secondary shield temperatures than tantalum and represent an attractive thermal material for making the secondary heat shields.

After analyzing the functional dependence of the temperature levels of the three secondary heat shields and of the spacecraft payload on the design variables α_i's and $D_{i,j}$'s and determining realistic emissivity values for S_1, S_2, and S_3, it is desirable to expand the range of variation in the α_i's as follows

$$\alpha_1=68° \text{ to } 112°, \quad \alpha_2=76° \text{ to } 120°, \quad \alpha_3=84° \text{ to } 128° \tag{14}$$

while the $D_{i,j}$ are given by Eq. (12). Figure 6 displays the temperature levels of S_1, S_2, S_3, and S_{SC} as a function of α_1 where the shaded area indicates the range of temperature variations as a function of α_2 and α_3 at a given α_1. It is evident from Fig. 6 that T_1 is strongly dependent upon α_1, with large values of α_1 yielding smaller T_1. It should also be noted that using smaller α_1, such as 80°, yields lower temperature levels of T_2, T_3 and T_{SC} when compared to Fig. 5. For constant α_1, one also concludes that minimum T_{SC} occurs for maximum difference $(\alpha_3-\alpha_2)$; minimum T_3 occurs for $(\alpha_2-\alpha_3)=(\alpha_2-\alpha_1)$; minimum T_2 occurs for maximum difference $(\alpha_2-\alpha_1)$; and minimum T_1 occurs for maximum α_1. It should also be noted there is a 60% reduction in T_{SC} when $\epsilon_{SC3}=\epsilon_{SC4}=0.85$ with smaller variations in T_1, T_2, and T_3 (1, 2, and 6%, respectively).

The general conclusion from this analysis of the system of three secondary heat shields is that the temperature levels of each surface are gradually increasing or decreasing functions of the design variables without any well defined "true minima," and thus, a design tradeoff of the STARPROBE spinner spacecraft as a whole must be considered before an optimum secondary heat shield system can be determined. Since T_{SC} is less than 200°K for many cases under consideration, an analysis of the feasibility of using two secondary heat shields is suggested.

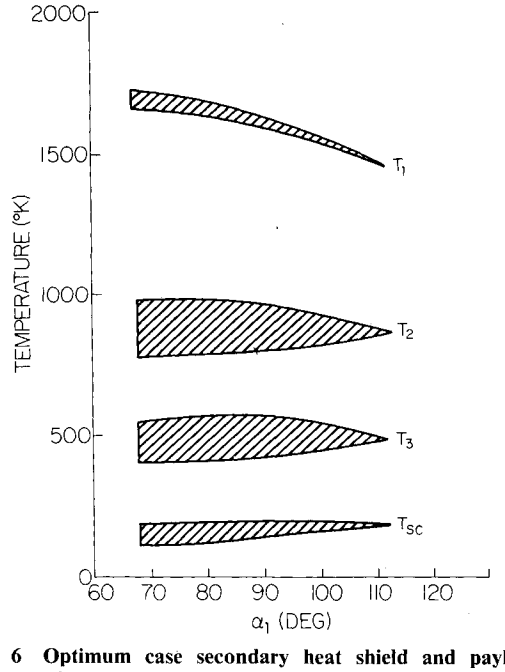

Fig. 6 Optimum case secondary heat shield and payload temperatures for configuration defined by Eqs. (12,13) vs α_1 when α_2 varied in the range of [76° − 120°] and α_3 varied[2] in the range of [84° − 128°].

Conclusions

A net-radiation method has been formulated such that the temperature levels of N secondary heat shields and payload of a spacecraft can be calculated in terms of the emissivities and the configuration factors between adjacent surfaces when the primary heat shield temperature is specified. For the case of conical secondary heat shields, a limited parametric study has been carried out when the cone half-angles, the intershield spaces, and emissivities are varied for systems of three secondary heat shields.

The general conclusion of the investigations is that temperature levels less than 300°K for the three secondary heat shield systems are, in fact, achievable. Using parametric thermal data for the secondary heat shield system, design tradeoff studies for the STARPROBE spinner spacecraft are required in order to establish an optimum secondary heat shield system. It should be further noted that in a real situation one would be unable to specify the primary shield temperature as has been assumed in this work. Rather, the problem is coupled in that the primary shield temperature would depend upon the incident radiation, its material, and its configuration as well as that of the secondary shields and the spacecraft. Also, in a more complete analysis, the thermal conductivity of the shield surfaces and the possibility of different emissivities on each side of a shield surface should be considered.

Appendix A

In this Appendix, a derivation of Eq. (5) will be given. Consider the symbolic diagram of the spacecraft heat shield system shown in Fig. 1 where the secondary shields view only adjacent surfaces and space. The energy balance equation at S_1 is then given by

$$2E_{b1}=G_1(+)+G_1(-) \tag{A1}$$

where

$$J_{HS}=\epsilon_{HS}E_{bHS}+\rho_{HS}G_{HS} \tag{A1a}$$

$$G_{HS}=F_{HS-1}J_1(+) \tag{A1b}$$

$$J_1(+)=\epsilon_1E_{b1}+\rho_1G_1(+) \tag{A1c}$$

$$G_1(+)=F_{1-HS}J_{HS} \tag{A1d}$$

$$J_1(-)=\epsilon_1E_{b1}+\rho_1G_1(-) \tag{A1e}$$

$$G_1(-)=F_{1-2}J_2(+) \tag{A1f}$$

$$J_2(+)=\epsilon_2E_{b2}+\rho_2G_2(+) \tag{A1g}$$

$$G_2(+)=F_{2-1}J_1(-) \tag{A1h}$$

Recall, that F_{i-j} is the configuration factor between S_i and S_j and is the fraction of energy emitted by S_i and incident upon S_j.

Combining Eqs. (A1a) and (A1d) and solving for $G_1(+)$ yields

$$G_1(+)=\frac{\epsilon_{HS}F_{1-HS}E_{bHS}+\epsilon_1\rho_{HS}F_{1-HS}F_{HS-1}E_{b1}}{1-\rho_1\rho_{HS}F_{1-HS}F_{HS-1}} \tag{A2a}$$

Similarly, combining Eqs. (A1e) and (A1h) yields

$$G_1(-)=\frac{\epsilon_2 F_{1\to 2}E_{b2}+\epsilon_1\rho_2 F_{1\to 2}F_{2\to 1}E_{b1}}{1-\rho_1\rho_2 F_{1\to 2}F_{2\to 1}} \tag{A2b}$$

Therefore, Eq. (A1) can be written as

$$M(1,1)E_{b1}+M(1,2)E_{b2}=N(1)E_{bHS} \tag{A3}$$

where

$$M(1,1)=2-\frac{\epsilon_1\rho_{HS}F_{1\to HS}F_{HS\to 1}}{1-\rho_1\rho_{HS}F_{1\to HS}F_{HS\to 1}}-\frac{\epsilon_1\rho_2 F_{1\to 2}F_{2\to 1}}{1-\rho_1\rho_2 F_{1\to 2}F_{2\to 1}} \tag{A3a}$$

$$M(1,2)=\frac{-\epsilon_2 F_{1\to 2}}{1-\rho_1\rho_2 F_{1\to 2}F_{2\to 1}} \tag{A3b}$$

$$N(1)=\frac{\epsilon_{HS}F_{1\to HS}}{1-\rho_1\rho_{HS}F_{1\to HS}F_{HS\to 1}} \tag{A3c}$$

Applying the energy balance condition at each surface i for $i=2,3,\ldots,N$ yields $N-1$ equations of the form

$$M(i,i-1)E_{bi-1}+M(i,i)E_{bi}+M(i,i+1)E_{bi+1}=0 \tag{A4}$$

where for $2\le i\le N-1$

$$M(i,i-1)=\frac{\epsilon_{i-1}F_{i\to i-1}}{1-\rho_{i-1}\rho_i F_{i\to i-1}F_{i-1\to i}}$$

$$M(i,i)=2-\frac{\epsilon_i\rho_{i-1}F_{i\to i-1}F_{i-1\to i}}{1-\rho_{i-1}\rho_i F_{i-2-1}F_{i-1\to i}}$$

$$-\frac{\epsilon_i\rho_{i+1}F_{i\to i+1}F_{1+1-1}}{1-\rho_i\rho_{i+1}F_{i-1+1}F_{1+1\to i}} \tag{A4b}$$

$$M(i,i+1)=\frac{-\epsilon_{i+1}F_{i\to i+1}}{1-\rho_i\rho_{i+1}F_{i\to i+1}F_{i+1\to i}} \tag{A4c}$$

and for $i=N$

$$M(N,N-1)=\frac{-\epsilon_{N-1}F_{N\to N-1}}{1-\rho_N\rho_{N-1}F_{N\to N-1}F_{N-1\to N}} \tag{A4d}$$

$$M(N,N)=2-\frac{\epsilon_N\rho_{N-1}F_{N\to N-1}F_{N-1\to N}}{1-\rho_N\rho_{N-1}F_{N\to N-1}F_{N-1\to N}} \tag{A4e}$$

$$-\frac{\epsilon_N[\rho_{SC1}F_{SC1\to N}F_{N\to SC1}+V]}{1-\rho_N[\rho_{SC1}F_{SC1-N}F_{N\to SC1}+V]} \tag{A4f}$$

$$M(N,N+1)=\frac{-[\epsilon_{SC1}F_{N\to SC1}+\epsilon_{SC2}F_{N-SC2}+\epsilon_{SC2}UF_{SC2\to SC2}]}{1-\rho_N[\rho_{SC1}F_{SC1-N}F_{N-SC1}+V]} \tag{A4g}$$

$$U=\frac{\rho_{SC2}F_{N-SC2}}{1-\rho_{SC2}F_{SC2-SC2}} \tag{A4h}$$

$$V=UF_{SC2-N} \tag{A4i}$$

Equations (A3) and (A4) are N linear equations in $N+1$ unknowns. The remaining equation follows from the energy balance condition at the spacecraft:

$$\epsilon_{SC1}A_{SC1}G_{SC1}+\epsilon_{SC2}A_{SC2}G_{SC2}=\left[\sum_{i=1}^{4}\epsilon_{SCi}A_{SCi}\right]E_{bSC} \tag{A5}$$

Equation (A5) is not exact, since the irradiation G_{SC3} has been assumed small in comparison with G_{SC1} or G_{SC2}, and, thus, neglected. Eliminating G_{SC1} and G_{SC2} from Eq. (A5) in a similar manner as was done for $G_1(\pm)$ in Eqs. (A1) and (A3) gives the result for energy balance condition at the spacecraft payload

$$M(N+1,N)E_{bN}+M(N+1,N+1)E_{bSC} \tag{A6}$$

where

$$M(N+1,N)=\epsilon_N W \tag{A6a}$$

$$M(N+1,N+1)=\rho_N W[\epsilon_{SC1}F_{N-SC1}+\epsilon_{SC2}F_{N\to SC2}$$

$$+\epsilon_{SC2}UF_{SC2\to SC2}]+\left[-\sum_{i=1}^{4}\epsilon_{SCi}A_{SCi}+\frac{\epsilon_{SC2}^2A_{SC2}F_{SC2\to SC2}}{1-\rho_{SC2}F_{SC2\to SC2}}\right]$$

$$\times\{1-\rho_N[\rho_{SC1}F_{SC1-N}F_{N-SC1}+V]\} \tag{A6b}$$

$$W=\epsilon_{SC1}A_{SC1}F_{SC1-N}+\frac{\epsilon_{SC2}A_{SC2}F_{SC2-N}}{1-\rho_{SC2}F_{SC2-SC2}} \tag{A6c}$$

Appendix B

In this Appendix, a brief summary of some important properies of configuration factors is given. Formulas for the configuration factors between the primary and secondary heat shields and the payload are then given.

1) Configuration factor between a finite, diffusely emitting area A_1 and a finite receiving area A_2

$$F_{1\to 2}=\frac{1}{A}\int_{A_1}\int_{A_2}\frac{\cos\beta_1\cos\beta_2}{\pi S_{12}^2}\,dA_1\,dA_2 \tag{B1}$$

where β_1 and β_2 are the angles between the surface normals and the line connecting dA_1 and dA_2. S_{12} is the distance between dA_1 and dA_2.

2) Reciprocity relationship

$$A_iF_{i-j}=A_jF_{j\to i} \tag{B2}$$

3) Enclosure relationship for the general case of N surfaces within the enclosure

$$\sum_{j=1}^{N}F_{i-j}=1, \qquad i=1,2,\ldots,N \tag{B3}$$

The term F_{i-i} is included in the summation of Eq. (B3) for a concave surface which can "see" part of itself. For a convexed surface i, $F_{i-i}=0$.

Now consider the STARPROBE spinner spacecraft, conical heat shield system shown in Figs. 1 and 2. Assuming S_1 and S_2 are arbitrary, adjacent shield surfaces, the configuration factor, F_{1-2} is defined by Eq. (B1). As a result of azimuthal symmetry of the heat shield system, the element of area dA_1 can be fixed at $(r_1,0,Z_1)$, where the origin of the coordinate system is on the symmetry axis at the base of payload. The coordinate of dA_2 are (r_2,ϕ_2,Z_2). Equation (B1) can then be written

$$F_{1\to 2}=C_1\int_{r_{1L}}^{r_{1U}}r_1\,dr_1\int_{r_{2L}}^{r_{2U}}r_2\,dr_2\int_0^{\phi_2^*}d\phi_2\frac{\cos\beta_1\cos\beta_2}{S_{12}^2} \tag{B4}$$

where

$$C_1=\frac{4}{\pi(r_{1U}^2-r_{1L}^2)\sin\alpha_2}$$

$$S_{12}^2=[r_2\cos\phi_2-r_1]^2+r_2^2\sin^2\phi_2$$

$$+[(Z_{0,2}-Z_{0,1})+(r_2\cot\alpha_2-r_1\cot\alpha_1)]^2 \tag{B4a}$$

$$\cos\beta_1 = \frac{1}{S_{12}}\{\cos\alpha_1(r_2\cos\phi_2 - r_1) - \sin\alpha_1[(Z_{0,2} - Z_{0,1}) + (r_2\cot\alpha_2 - r_1\cot\alpha_1)]\} \quad \text{(B4b)}$$

$$\cos\beta_2 = \frac{1}{S_{12}}\{\cos\alpha_2(r_2 - r_1\cos\phi_2) - \sin\alpha_2[(Z_{0,2} - Z_{0,1}) + (r_2\cot\alpha_2 - r_1\cot\alpha_1)]\} \quad \text{(B4c)}$$

when S_1 is the primary heat shield, r_{1L} and r_{1U} are the inner and outer radii of the primary shield and are given by

$$r_{1L} = r_{HS} \quad 0.711 \text{ m. (28 in.)}$$
$$r_{1U} = R_{HS} \quad 2.032 \text{ m. (80 in.)} \quad \text{(B5)}$$

On the other hand, if S_1 is a secondary heat shield, then r_{1L}, r_{1U} are determined such that S_1 remains within the shadow cone of the primary heat shield. In order to determine r_{iL} and r_{iU} for the ith secondary shield surface, it is necessary to solve simultaneously the equation of S_i with the equation of the inner and outer shadow cones respectively

$$R_{i,L} = \frac{r_{i-1,L}[1 + \tau\cot\alpha_{i-1}] - \tau[Z_{0,i} - Z_{0,i-1}]}{1 - \tau\cot\alpha_i} \quad \text{(B6)}$$

and

$$r_{i,U} = \frac{r_{i-1,U}[1 - \tau\cot\alpha_{i-1}] + \tau[Z_{0,i} - Z_{0,i-1}]}{1 - \tau\cot\alpha_i} \quad \text{(B7)}$$

where $\tau = \tan\beta_{\text{sun}}$ and $r_{i-1,U}$ are known. Now evaluate the angular limit of integration over S_2. If S_1 is the primary heat shield, then ϕ_2^* for a given r_2 is determined by the loci of points of the intersection of the tangent plane to dA_1 and the surface S_2:

$$\phi_2^* = \arccos\left[\frac{(Z_{0,2} - Z_{0,1}) + r_2\text{co} + \alpha_2}{r_2\cot\alpha_1}\right] \quad \text{(B8)}$$

If on the other hand, S_1 is a secondary shield, then ϕ_2^* is determined such that a vector from dA_1 to dA_2 is perpendicular to the normal vector at dA_2:

$$\phi_2^* = \arccos\left[\frac{(Z_{0,1} - Z_{0,2}) + r_1\cot\alpha_1}{r_1\cot\alpha_2}\right] \quad \text{(B9)}$$

Equations (B4) through (B9) are used to compute the configuration factors between adjacent shield surfaces. The coefficients in Eq. (5) are also expressed in terms of the configuration factors between the last heat shield S_N and the payload surfaces S_{SC1} and S_{SC2}. Figure B1 illustrates the geometry under consideration. Using the same technique which gave Eq. (B4), it follows that the configuration factor between S_N and S_{SC1} is given by

$$F_{N-SC1} = C_N\int_{r_{NL}}^{r_{NU}} r_N f(r_N)\,dr_N \quad \text{(B10)}$$

where

$$C_N = \frac{2}{\pi(r_{NU}^2 - r_{NL}^2)} \quad \text{(B10a)}$$

$$f(r_N) = \int_0^{2\pi}\int_{r_{SC}}^{R_{SC}} \frac{\cos\beta_N\cos\beta_{SC1}}{S_{N-SC1}^2} r_{SC1}\,dr_{SC1}\,d\phi_{SC1} \quad \text{(B10b)}$$

$$S_{N-SC1}^2 = [r_{SC}\sin\phi_{SC2} - r_N]^2 + r_{SC}^2\sin^2\phi_{SC2} + [Z_{SC2} - Z_N(r_N)]^2 \quad \text{(B10c)}$$

$$\cos\beta_N = \frac{1}{S_{N-SC1}}\{\cos\alpha_n[r_{SC1}\cos\phi_{SC1} - r_N] - \sin\alpha_N[H_{SC} - Z_N]\} \quad \text{(B10d)}$$

$$\cos\beta_{SC1} = [Z_N(r_N) - H_{SC}]/S_{N-SC1} \quad \text{(B10e)}$$

and the configuration factor between S_N and S_{SC2} is given by

$$F_{N-SC2} = 2r_{SC}C_N\int_{r_{NL}}^{r_{NU}} r_N g(r_N)\,dr_N \quad \text{(B11)}$$

where

$$g(r_N) = \int_0^{H_S}\int_{\phi_{SC2}^*}^{\pi} \frac{\cos\beta_N'\cos\beta_{SC2}}{S_{N-SC2}^2} d\phi_{SC2}\,dZ_{SC2} \quad \text{(B11a)}$$

$$S_{N-SC2}^2 = [r_{SC}\cos\phi_{SC2} - r_N]^2 + r_{SC}^2\sin^2\phi_{SC2} + [Z_{SC2} - Z_N(r_N)]^2 \quad \text{(B11b)}$$

$$\cos\beta_N' = \frac{1}{S_{N-SC2}}\{\cos\alpha_N[r_{SC}\cos\phi_{SC2} - r_N] - \sin\alpha_N[Z_{SC2} - Z_N(r_N)]\} \quad \text{(B11c)}$$

$$\cos\beta_{SC2} = [r_{SC} - r_N\cos\phi_{SC2}]/S_{N-SC2} \quad \text{(B11d)}$$

The angular limit ϕ_{SC2}^* is determined empirically by a ray tracing technique such that no blockage of S_{SC2} due to S_{SC1} occurs when dA_{SC2} is viewed from dA_N.[19] Varying ϕ_{SC2} from 180 to 0 deg in small increments, the radial intercepts R_D with plane $Z = H_{SC}$ of a line connecting dA_N and dA_{SC2} are evaluated. The lower angular limit ϕ_{SC2}^* is the largest value of ϕ_{SC2} for which R_D is greater than r_{SC}.

The remaining configuration factor, $F_{SC2-SC2}$, needed to solve the system of Eq. (5) is given by

$$F_{SC2-SC2} = \frac{1}{\pi H_{SC}}\int_0^{H_{SC}} h(Z_1)\,dZ_1 \quad \text{(B12)}$$

where

$$h(Z_1) = \int_0^{H_{SC}}\int_0^{2\pi} \frac{r_{SC}^2(1 - \cos\phi_2)^2\,d\phi_2}{[2r_{SC}^2(1 - \cos\phi_2) + (Z_2 - Z_1)^2]^2} \quad \text{(B13)}$$

Using the reciprocity relationship given by Eq. (B2), one can evaluate the remaining configuration factors required to specify all the coefficients in Eq. (5).

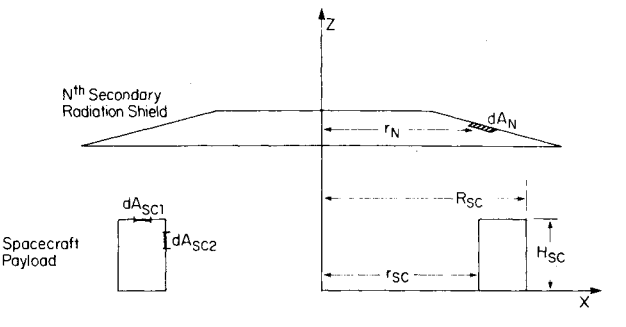

Fig. B1 Symbolic view of the x-z cross-section of the Nth secondary radiation shield and the payload.

Acknowledgment

The author would like to acknowledge useful comments from J.M. Millard, R.N. Miyake, J.H. Lundell, and H. Figueroa during the preparation of this manuscript. This study was funded in part by the Jet Propulsion Laboratory, California Institute of Technology, Contract No. 956086.

References

[1] Roth, E.A., "Solar Probe," *International Symposium on Exploration fo the Planetary System,* Paper No. 78-014, Munich, West Germany, April 1978.

[2] Neugebauer, M. and Davies, R.W., "A Close-up of the Sun," Jet Propulsion Laboratory, Pasadena, Calif., Report No. 78-70, Sept. 1978.

[3] Bender, D.B., Neugebauer, M., Randolph, J.E., and Yen, C.L., "Preliminary Mission Design Studies for the Close Solar Probe Mission," *Astrodynamics Conference,* AIAA/AAS, Paper No. 78-1440, Aug. 1978.

[4] Randolph, J.E., "A Solar Encounter Mission-STARPROBE," XXXI Congress, International Astronautical Federation, 80-G294, Sept. 1980.

[5] Hurick, M.G., 'STARPROBE Primary Thermal Sheld Design Requirements Document," Jet Propulsion Laboratory, Pasadena, Calif., Report No. 715-79, Feb. 1981.

[6] Park, C., "Preliminary Design Study of Solar Probe Heat Shields," *Proceedings: AIAA 19th Aerospace Science Meeting,* Paper No. 81-0352, St. Louis, Mo., Jan. 1981.

[7] Anon., "Close Approach Solar Probe," AVCO Technical Report RAD-TR-63-35, Sept. 1963.

[8] Lundell J.H., "Graphitic Heat Shields for the Solar Probe Missions," *16th Thermophysics Conference,* AIAA Paper 81-1056, Palo Alto, Calif., June 1981.

[9] Randolph, J.E., "Solar Probe Final Report of 1979," Jet Propulsion Laboratory, Pasadena, Calif., Report No. 715-5, Dec. 1979.

[10] Randolph, J.E., "Solar Probe Midyear Status Report-1980," Jet Propulsion Laboratory, Pasadena, Calif., Report No. 715-44, June 1980.

[11] Siegel, R. and Howell, J.R., *Thermal Radiation Heat Transfer,* McGraw-Hill, New York, 1972, pp. 236-273.

[12] Keith, F. and Black, W.Z. , *Basic Heat Transfer,* Harper & Row, New York, 1980, pp. 325-346

[13] Thomas, L.C., *Fundamentals of Heat Transfer,* Prentice-Hall, Englewood Cliffs, N.J., 1980, pp. 273-309.

[14] Holman, J.P., *Heat Transfer,* McGraw-Hill, New York, 1968, pp. 239-242.

[15] Emslie, A.G., and String, P.F., "Passive Temperature Control in Radiation Environments," *Radiative Transfer from Solid Materials,* edited by Blay and Fishier, H. Blau and H. Fisher, Macmillian, New York, 1962, p. 234-247.

[16] *International Mathematical & Statistical Libraries,* 8th Ed., Houston, Texas, 1980, Subroutine LEQTIF.

[17] Bobco, R.P., "Radiation Heat Transfer in Semigray Enclosures with Specularly and Diffusely Reflecting Surfaces," *Journal of Heat Transfer,* Transactions of the ASME, Series C., Vol. 86, 1964, pp. 123-129.

[18] Gebhart, B., "Surface Temperature Calculations in Radiant Surrounds of Arbitrary Complexity for Gray Diffuse Radiation," *International Journal of Heat and Mass Transfer,* Vol. 3, 1961, pp. 341-346.

[19] Shealy, D.L., "An Analysis of the Infrared Radiation Shields for the STARPROBE Spinner Spacecraft," University of Alabama, Birmingham, Birmingham, Ala., Contract No. 95086, Sept. 1981.

[20] System/360 Scientific Subroutine Package, 4th Ed., International Business Machines, White Plains, New York, 1968, pp. 299-302.